Electronic Supporting Information

Facile self-templating synthesis of heteroatom-doped 3D porous carbon materials from waste biomass for supercapacitors

Yong Yao,‡[ab] Qiaoxia Feng,‡[ab] Baoyu Huo,[c] Haihui Zhou,*[ab] Zhongyuan Huang,*[ab] Huanxin Li,[ab] Zhanheng Yan,[ab] Xinxin Yang[ab] and Yafei Kuang*[ab]

[a] *State Key Laboratory for Chemo/Biosensing and Chemometrics, College of Chemistry and Chemical Engineering, Hunan University, Changsha, 410082, China.*

[b] *Advanced Catalytic Engineering Research Center of the Ministry of Education, Hunan University, Changsha, 410082, China*

[c] *Mud Technical Service Branch of Bohai Drilling Engineering Limited Company, China National Petroleum Corporation, Tianjin, 300450, China*

* E-mail: haihuizh@163.com, zhongyhuang@hnu.edu.cn and yafeik@163.com.

‡ These two authors have the same contribution to this paper.

List of Contents:

1.Experimental Section

Synthesize of the PBC. Firstly, the pig bones were washed with deionized water for three times and then dried at 80 °C for 24 hours. Then the pig bones were crushed into fine powders and calcined at 800 °C for 2 hours with a heating rate of 5 °C min^{-1} under the N_2 atmosphere. The calcined pig bone carbon without treatment of dilute nitric acid was marked as PBC.

Synthesize of the PPBC. The calcined pig bone carbon was mixed with 2 M nitric acid at room temperature for 8 hours under magnetic agitation, and the used dilute nitric acid can be collected for reusing. Finally, the resultant samples were washed with deionized water until the filtrate was neutral and dried at 80 °C for 12 hours. The obtained porous pig bone carbon was denoted as PPBC.

Material Characterizations. Scanning electron microscope (SEM) (Hitachi S-4800, Japan) and transmission electron microscopy (TEM, JEM-3100F, Japan) under different magnifications were performed to investigate the morphology of the composite materials. The composition of phase and crystal structure was confirmed by an X-ray diffractometer (XRD, Rigaku, D/max-2200pc) with Cu Ka radiation (l ¼ 0.15406 nm) between 10° and 80° with a scan rate of 8° min^{-1}. To further investigate the microstructures of materials, Raman scattering (Lab Ram HR800) was applied. Fourier transform infrared spectroscopy (FTIR, NICOLET iS10)

was used to characterize the surface functional groups of all samples. To obtain the element information, X-ray photoelectron spectroscopy (XPS) analysis was performed on ESCALAB 250 with monochromatic Al Kα X-ray sources. To get the surface area and porosity informations of the samples, Brunauer-Emmett-Teller (BET) surface area measurements were conducted by nitrogen adsorption and desorption method using an ASAP 2460 Analyzer (Mac, America).

Electrochemical measurements in a three-electrode system. In a typical three-electrode system, a platinum foil, an Hg/HgO electrode and 6 M KOH were used as counter electrode, reference electrode and electrolyte, respectively. The glassy carbon electrode was acted as a working electrode with 25 mL of suspension (2 mg mL^{-1}) of sample spread evenly over the top. And 10 mL of Nafion solution (in deionized water solution at a mass ratio of 1:200) was used to fix the sample. The cyclic voltammetry (CV), galvanostatic charge/discharge (GCD) and electrochemical impedance spectroscopy (EIS) curves were performed on a CHI660E electrochemical workstation (Shanghai Chenhua Instrument Co., China). The potential window of the CV and GCD curves was -1.0 V – 0 V. The EIS curves were tested in the frequency range from 10^5 Hz to 10^{-2} Hz at the open circuit potential with the amplitude of 5 mV. In the three-electrode system, the specific capacitance C (F g^{-1}) of samples was calculated from the GCD curves by the following equation (1) and (2):[1]

$$E_{int} = I \cdot \int_{t(U_{max})}^{t(U_{min})} U(t)dt \quad (1)$$

$$C = \frac{E_{int}}{m \cdot U_{max}^{2}} \quad (2)$$

Where E_{int} is discharge energy (W•s), I is discharge current (A), U_{max} (V) and U_{min} is the maximum and minimum voltage during discharge process (V), respectively, $t(U_{max})$ and $t(U_{min})$ is corresponding time of maximum and minimum voltage during discharge process (s), severally, m is the mass of active material on the electrode (g).

Electrochemical measurements in a two-electrode system. The electrochemical testing of the supercapacitors in the symmetric two-electrode system was conducted with a coin-cell (CR2025) configuration. The carbon paper and filter paper were used as a collecting fluid and diaphragm, respectively, 6 M KOH and 0.8 M KPF_6 (in an EC/DEC solution at a volume ratio of 1:1) were used as electrolytes, severally. The working electrode was prepared by mixing the carbon samples, polytetrafluoroethylene (PTFE) and acetylene black in a weight ratio of 80 : 10 : 10. The active material mass of single film was about 1.3 ~ 2.0 mg cm^{-2}. The CV, GCD and EIS measurements were carried out with a CHI660E electrochemical workstation (Shanghai Chenhua Instrument Co., China). The potential window of the CV and GCD was 0 – 1.2 V in 6 M KOH and 0 ~ 5.0 V in 0.8 M KPF_6. The EIS curves were tested in the

frequency range from 10^5 Hz to 10^{-2} Hz at the open circuit potential with the amplitude of 5 mV. In the symmetric two-electrode configuration, the specific capacitance C (F g^{-1}), the energy density E (W h kg^{-1}) and the power density P (W kg^{-1}) was calculated by the following equation (3) (4) and (5):[1]

$$C = \frac{2 \cdot E_{int}}{m \cdot U_{max}^{2}} \tag{3}$$

$$E = \frac{E_{int}}{3.6 \cdot m} \tag{4}$$

$$P = \frac{E}{\Delta t} \tag{5}$$

Where E_{int} represents discharge energy (W•s), m represents the mass of active material on the electrode (g), and Δt represents the discharge duration time (s).

2.Supplementary Tables and Figures

Table S1 The mass percentages of different elements in PBC and PPBC.

	C	Ca	O	P	N
PBC	50.25%	8.92%	31.50%	6.38%	2.95%
PPBC	75.02%	0.17%	18.14%	0.30%	6.36%

The mass percentages of different elements in PBC and PPBC were also tested by XPS, as shown in Table S1. It can be seen that the contents of Ca, O and P in PBC are 8.92%, 31.50% and 6.38%, respectively, while the contents of Ca, O and P in PPBC are only 0.17%, 18.14% and 0.30%. Consequently, the contents of Ca, P and O atoms in PPBC are greatly reduced after dilute nitric acid etching. These results confirm the successful removal of hydroxyapatite in pig bones. At the same time, it can be seen that the contents of C and N atoms in PPBC are up to 75.02% and 6.36%, which are higher than those in PBC (50.25% and 2.95%). It shows that the mass percentage of nitrogen atoms in PPBC was increased after etching by HNO_3.

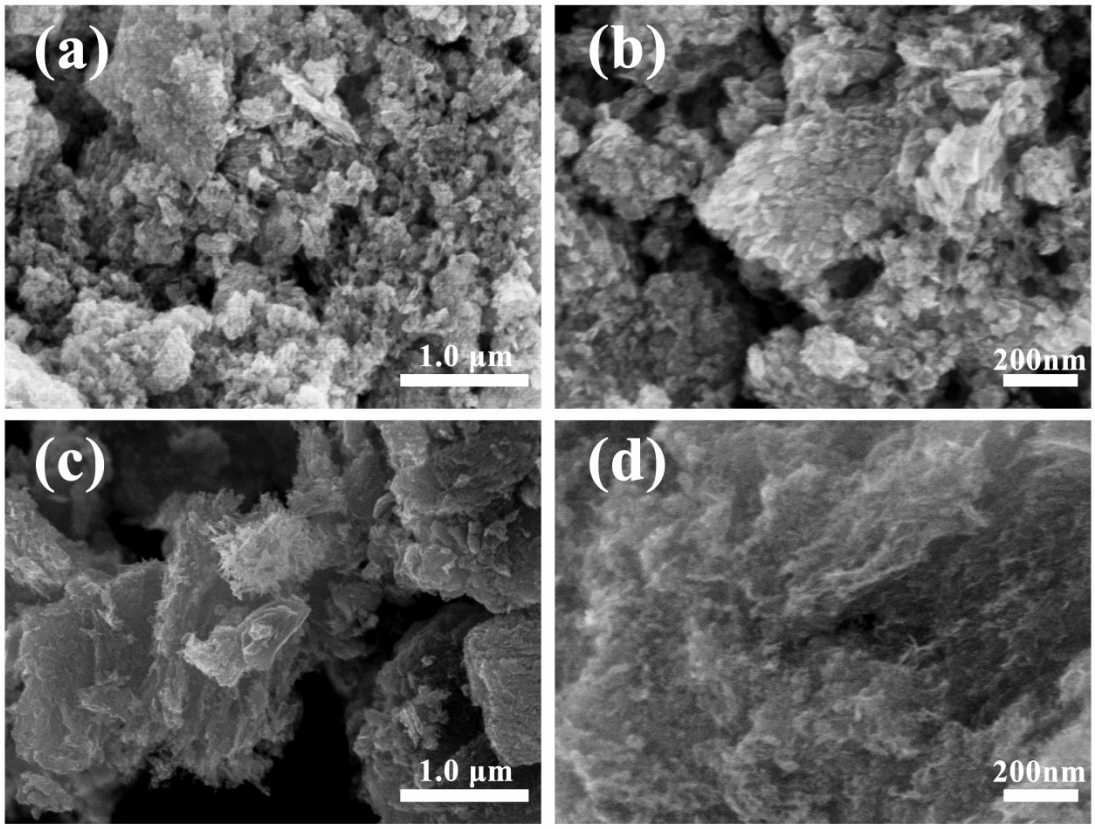

Fig. S1 SEM images of (a) ~ (b) PBC and (c) ~ (d) PPBC at different magnifications.

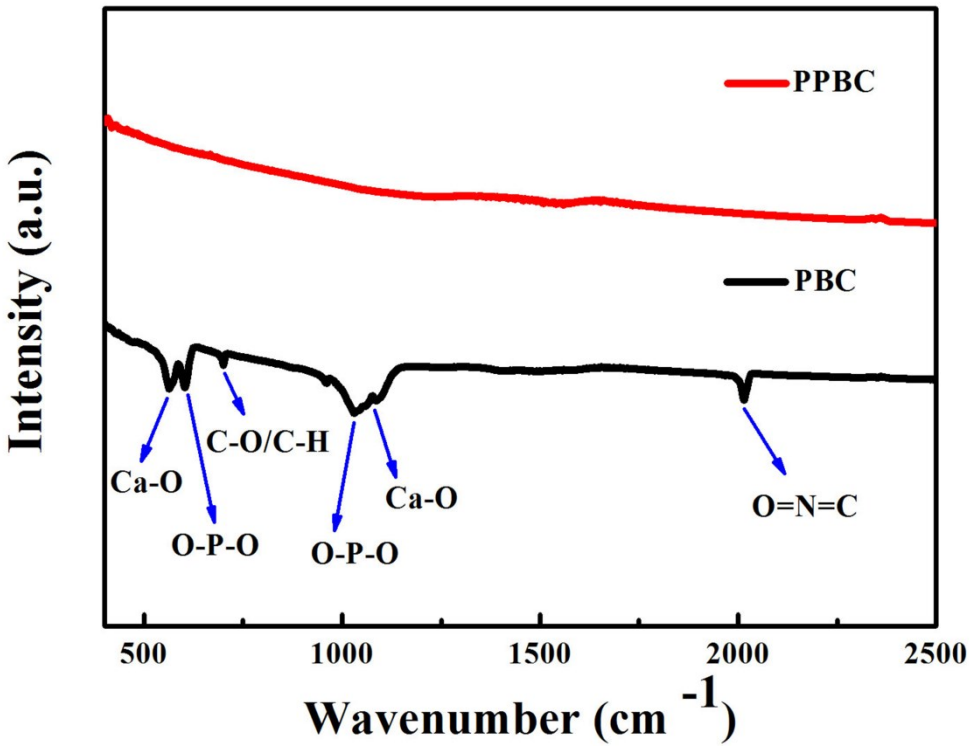

Fig. S2 FTIR results of PBC and PPBC.

The FTIR patterns of PBC and PPBC are shown in Fig S2. The FTIR result of PBC shows the typical peaks of Ca-O bond (~566 cm^{-1} and ~1090 cm^{-1}) [2] and O-P-O bond (~600 cm^{-1} and ~1050 cm^{-1})[3], indicating the presence of hydroxyapatite. In addition, the peaks at ~702 cm^{-1} and ~2100 cm^{-1} are also observed, which are attributed to C-O/C-H and O=N=C bonds.[2,4] However, above peaks almost completely disappeared in the FTIR result of PPBC, which further demonstrates that the hydroxyapatite was successfully removed.

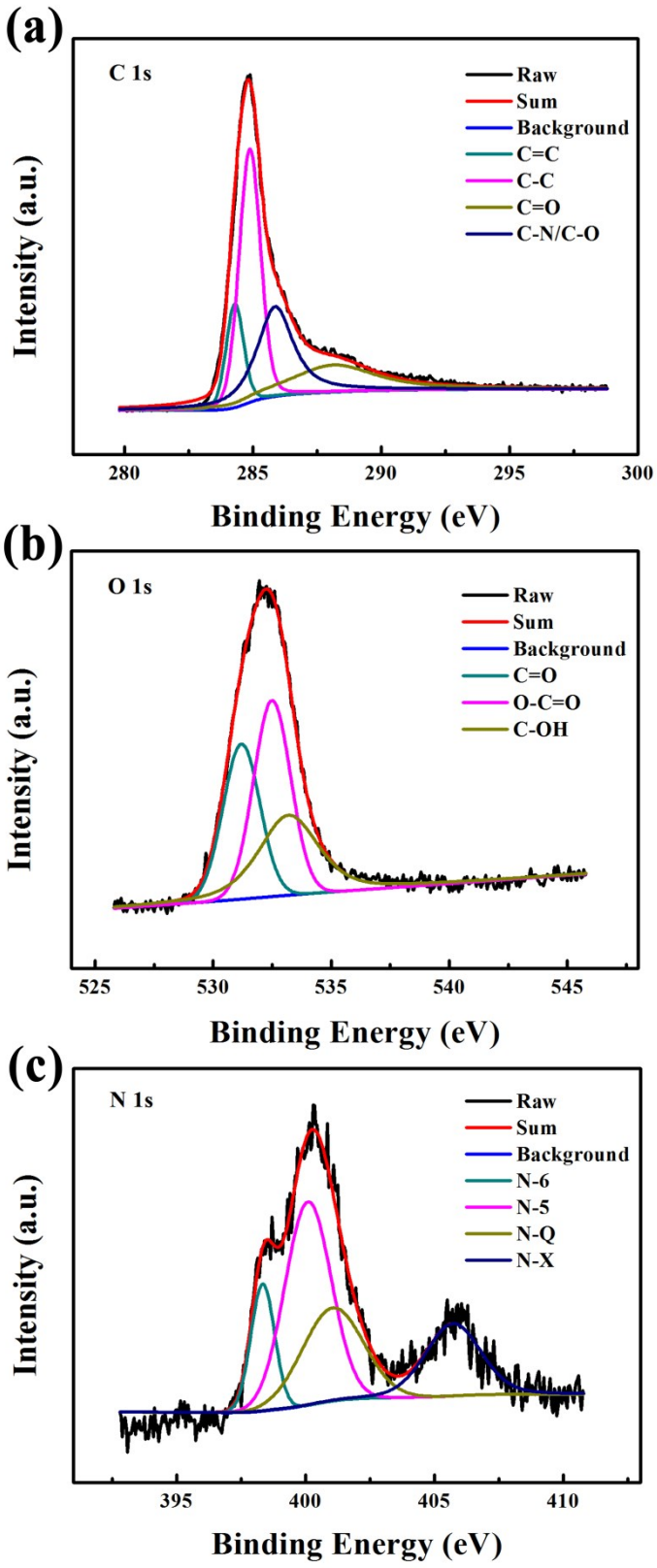

Fig. S3 XPS spectra of PPBC: (a) C 1s; (b) O 1s; (c) N 1s.

Table S2 Comparison of supercapacitive properties of PPBC with those of previously reported carbon materials in a three-electrode configuration.

Carbon Precursor	**Electro-lyte**	**Rate Performance ($F\ g^{-1}$)**			**Cycling Retention**	**Ref.**
		1 $A\ g^{-1}$	20 $A\ g^{-1}$	100 $A\ g^{-1}$		
Pig bones	**6 M KOH**	**484.01**	**290.85**	**217.27**	**99.97% after 10 k cycles at 10 $A\ g^{-1}$**	**This Work**
Bamboo char	6 M KOH	171.4	115.0	--	-	[5]
Salvia splendens	6 M KOH	294.0	--	--	--	[6]
Fish scale	6 M KOH	306	--	--	100% after 20 k cycles at 5 $A\ g^{-1}$	[7]
Cotton	6 M KOH	278	248	208	94.3% after 100 k cycles at 100 $A\ g^{-1}$	[8]
Polyacrylonitr-ile	6 M KOH	--	319	--	96.5% after 10 k cycles at 5 $A\ g^{-1}$	[9]
Tannic acid	1 M H_2SO_4	460.4	286.0	--	76.0% after 5 k cycles at 20 $A\ g^{-1}$	[10]
Sodium ligninsulfonate	1 M H_2SO_4	480	--	--	96.6% after 2 k cycles at 10 $A\ g^{-1}$	[11]
Bamboo leaves	3 M KOH	231	--	--	99% after 10 k cycles at 1 $A\ g^{-1}$	[12]

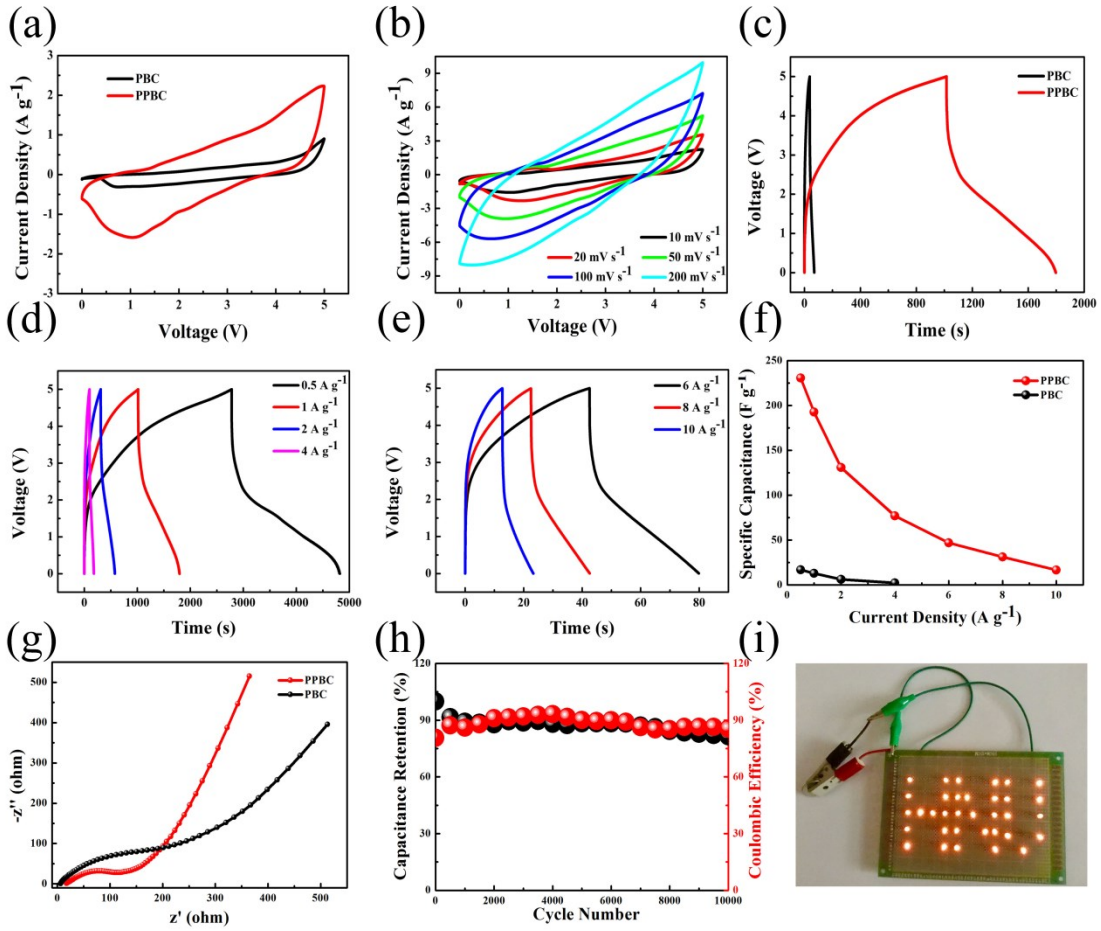

Fig. S4 Electrochemical performances in 0.8 M KPF_6 of the materals in a symmetrical capacitor configuration: (a) CV curves of PBC and PPBC at 10 mV s^{-1}; (b) CVs of PPBC at different scan rates from 10 mV s^{-1} to 200 mV s^{-1}; (c) GCD curves of PBC and PPBC at a current density of 1 A g^{-1}; (d) GCD curves of PPBC at different current densities from 0.5 A g^{-1} to 4 A g^{-1}; (e) GCD curves of PPBC at different current densities from 6 A g^{-1} to 10 A g^{-1}; (f) Specific capacitances of PBC and PPBC at different current densities from 1 A g^{-1} to 100 A g^{-1}; (g) Nyquist plots of PBC and PPBC; (h) Cycling stability and columbic efficiency of PPBC at 2 A g^{-1} after 10 000 cycles; (i) A symmetrical supercapacitor with organic electrolyte lights up 34 red LED bulbs to form a "HNU" pattern.

To further explore the practical application, symmetrical supercapacitors, PBC and PPBC, were assembled using 0.8 M KPF_6 as the

electrolyte, the obtained samples illustrate excellent electrochemical properties as well. The detailed information can be found in Fig. S4–S6. To our surprise, the working voltage range reaches an astonishing value (0–5.0 V) in 0.8 M KPF_6, which is larger than that in almost all the aqueous electrolytes, organic electrolytes and ionic liquid electrolytes and immensely increases the energy density of the symmetrical supercapacitors. As shown in Fig. S4a and S4b, the CV curves of PPBC still remained similarly rectangular shape with soft distortion, further confirming the pseudo-capacitance from the heteroatoms-doping. Additionally, in Fig. S4a, the current density of PBC is lower than that of PPBC and the CV curve of PBC represents an asymmetric shape, illustrating that PPBC has better capacitance performance than PBC. In Fig. S4b, the CV curves of PPBC at various scan rates of 10 mV s^{-1}, 20 mV s^{-1}, 50 mV s^{-1}, 100 mV s^{-1} and 200 mV s^{-1} maintain a relatively symmetrical rectangular shape, indicating its excellent rate performance in organic electrolyte.[13] As is shown in Fig. S4c ~ S4e, the GCD curves of PPBC show curved and asymmetric shapes, attributed to the faraday reactions and pseudocapacitive contributions induced by heteroatoms. Besides, the corresponding capacitance values of PPBC and PBC from GCD curves are shown in Fig. S4f. As can be seen from Fig. S4f, PPBC delivers high specific capacitances of 230.68 F g^{-1}, 192.78 F g^{-1}, 130.92 F g^{-1}, 77.06 F g^{-1}, 46.86 F g^{-1}, 31.19 and 16. 78 F g^{-1} at current densities of 0.5 A g^{-1}, 1 A

g^{-1}, 2 A g^{-1}, 4 A g^{-1}, 6 A g^{-1}, 8 A g^{-1} and 10 A g^{-1}, respectively. However, the capacitance values of PBC only are 16.82 F g^{-1}, 12.88 F g^{-1}, 6.37 F g^{-1} and 2.23 F g^{-1} at current densities of 0.5 A g^{-1}, 1 A g^{-1}, 2 A g^{-1} and 4 A g^{-1}. Thus we can conclude that the unique three-dimensional porous structure and abundant heteroatoms of PPBC enhanced its electrochemical properties. From the EIS results in Fig. S4g, approximately semicircular shapes in the high frequency region and slightly sloping lines in the low frequency region of PBC and PPBC are observed. The diameter of the semicircle relates to the charge transfer resistance (R_{CT}).[14] As can be seen from Fig. S4g, the diameter of PPBC is smaller than that of PBC, representing that PPBC has a lower impedance and diffusion resistance compared with PBC. Due to the extremely high operating voltage window (0 ~ 5.0 V), the maximum energy density of PPBC reaches 400.46 W h kg^{-1} at a power density of 144.05 W kg^{-1} and it retains 29.1 W h kg^{-1} at a power density of 3190.51 W kg^{-1}. As shown in Fig. S5, the energy density of PPBC is much higher than that of other reported carbon materials in ionic liquid or organic electrolytes. The PPBC demonstrates superb cycling stability at a current density of 2 A g^{-1} in organic electrolyte as shown in Fig. S4h. Its specific capacitance maintains 81.48% of its initial capacitance and the coulomb efficiency remains 85.48% after 10 000 cycles, indicating admirable long-term cycling stability and reversible capacity. Table S3 shows that even compared with other reported

symmetrical supercapacitors in ionic liquid or organic electrolyte, the as-prepared sample in this work also displays superior or competitive electrochemical properties. Fig. S4i displays a practical example, a "HNU" pattern formed by 34 red LED bulbs (operating voltage of each bulb is 2.1 V – 2.4 V and the power of each bulb is 0.06 W) is lighted up for 5 – 10 minutes by only one symmetrical supercapacitor in organic electrolyte, indicating that the heteroatoms-doped three-dimensional porous carbon materials have superb application prospect in supercapacitors. These results illustrate that the mesoporous structure and heteroatoms-doping of carbon materials play an important role in improving the performance of supercapacitors.

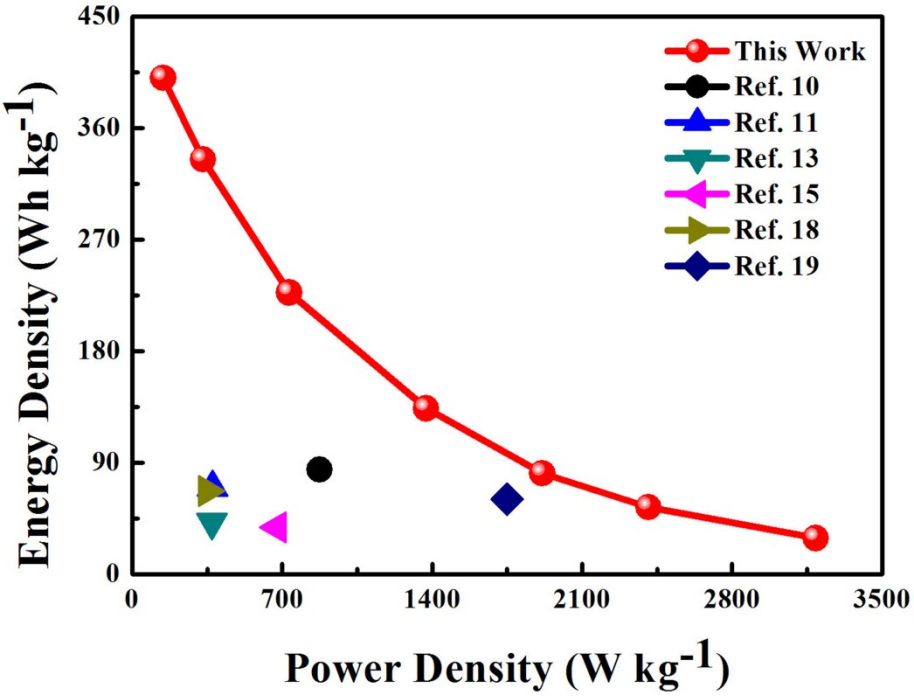

Fig. S5 Comparison of the energy density of the symmetric supercapacitor in organic electrolyte with that of other reported carbon materials in organic or ionic liquid electrolyte.

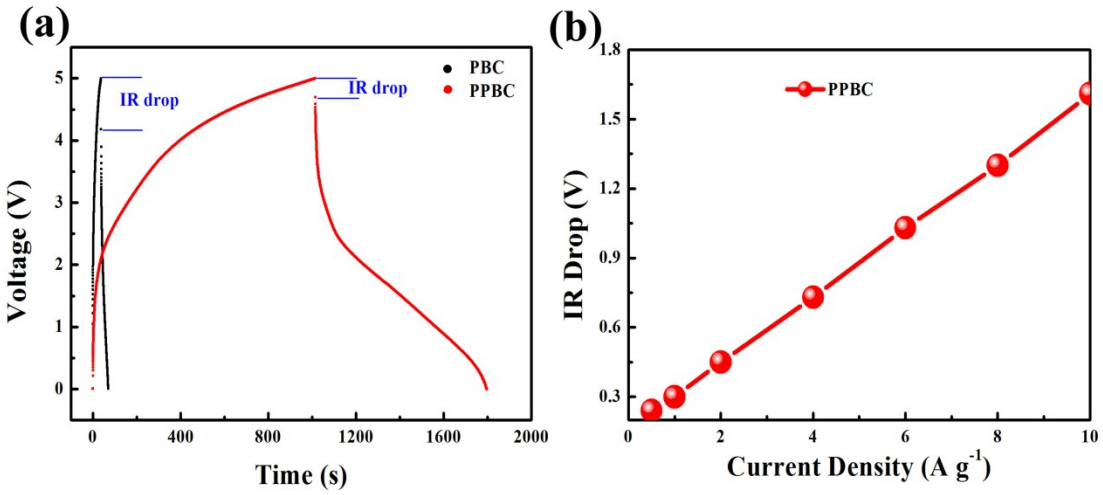

Fig. S6 (a) IR drops of PBC and PPBC in organic electrolyte at 0.5 A g^{-1}; (b) IR drops of PPBC in organic electrolyte at different current densities from 0.5 A g^{-1} to 10 A g^{-1}.

Generally speaking, the IR drop at the initial position of the discharge curves can be used to indicate the internal resistance of the electrolyte and electrodes.[15] In Fig. S6(a), the IR drop of PBC is 0.81 V at 0.5 A g^{-1}, which is higher than that of PPBC (0.24 V), suggesting that PBC has larger internal resistance. From Fig. S6(b), it can be clearly seen that IR drops of PPBC increase gradually from 0.24 V to 1.61 V with the current densities increase from 0.5 A g^{-1} to 10 A g^{-1}. In addition, the variation of IR drops in Fig. S6(b) show a linear relationship with the current densities, indicating the excellent fast-charging property.[16, 17]

Table S3 Comparison of supercapacitive properties of PPBC as symmetric supercapacitor with those of previously reported carbon materials in organic or ionic liquid electrolyte.

Electrode Material	Electro-lyte	Volta-ge (V)	Specific Capacitance	Cycle Stability	Ref.
PPBC	**0.8 M KPF_6**	**0 ~ 5.0**	**230.68 F g^{-1} at 0.5 A g^{-1}**	**81.48% retention after 10 k cycles**	**This work**
Microporous covalent triazine framework	$EMIMBF_4$	0 ~ 3.5	100 F g^{-1} at 0.1 A g^{-1}	92% retention after 5,000 cycles	[18]
Carbon nanomesh	$EMIMBF_4$	0 ~ 3.5	194 F g^{-1} at 1 A g^{-1}	90.6% retention after 10 k cycles	[19]
Covalent Triazine Framework	$LiPF_6$	0 ~ 3.0	251 F g^{-1} at 0.5 A g-1	89.0% retention after 20 k cycles	[20]
Carbon nanosheets	$TEABF_4$/AN	0 ~ 2.0	134 F g^{-1} at 5 A g-1	94% retention after 10 k cycles	[21]
Activated carbon	TEA-BF_4/AN	0 ~ 3.0	163 F g^{-1} at 0.5 A g-1	90.3% retention after 10 k cycles	[22]
N-Carbon nanosheets	$EMIMBF_4$	0 ~ 3.5	242 F g^{-1} at 0.1 A g^{-1}	92% retention after 10 k cycles	[23]
Mesopore carbon nanomesh	$TEABF_4$/AN	0 ~ 2.7	149 F g^{-1} at 1 A g^{-1}	99% retention after 5 k cycles	[24]
Graphene/carbonized metal-organic frameworks	$EMIMBF_4$/ PC	0 ~ 3.0	397 F g^{-1} at 1 A g^{-1}	98% retention after 60 k cycles	[25]
Ternary nanocomposite Gr/Co_3O_4/ PPy (GCP)	TEA-BF_4/ acetonitrile	-1~1	33.06 F g^{-1} at 10 mV s^{-1}	--	[26]
Porous sheet-like nanocarbons	$EMIMBF_4$	0 ~ 3.5	39.5 F g^{-1} at 0.2 A g^{-1}	88% retention after 5 k cycles	[13]
Carbon nanosheets framework	$EMIMBF_4$	0 ~ 3.5	~ 65 F g^{-1} at 1 A g^{-1}	88.5% retention after 5 k cycles	[27]

3. References

1. Y. Huang, J. Zhou, N. Gao, Z. Yin, H. Zhou, X. Yang and Y. Kuang, *Electrochimica Acta*, 2018, **269**, 649-656.
2. Y. Sun, G. Yang and L. Zhang, *Ecological Engineering*, 2018, **115**, 139-148.
3. M. D. O'Donnell, P. L. Candarlioglu, C. A. Miller, E. Gentleman and M. M. Stevens, *Journal of Materials Chemistry*, 2010, **20**.
4. S. Liu, J. Liu, G. Liu, Y. Liu and H. Zhong, *Applied Surface Science*, 2020, **505**.
5. Y. Gong, D. Li, C. Luo, Q. Fu and C. Pan, *Green Chemistry*, 2017, **19**, 4132-4140.
6. B. Liu, M. Yang, H. Chen, Y. Liu, D. Yang and H. Li, *Journal of Power Sources*, 2018, **397**, 1-10.
7. M. Liu, J. Niu, Z. Zhang, M. Dou and F. Wang, *Nano Energy*, 2018, **51**, 366-372.
8. W. Jiang, L. Li, J. Pan, R. A. Senthil, X. Jin, J. Cai, J. Wang and X. Liu, *Journal of Power Sources*, 2019, **438**, 226936.
9. S. Wang, Z. Xiao, S. Zhai, H. Wang, W. Cai, L. Qin, J. Huang, D. Zhao, Z. Li and Q. An, *Journal of Materials Chemistry A*, 2019, **7**, 17345-17356.
10. C. Xiong, Y. Zou, Z. Peng and W. Zhong, *Nanoscale*, 2019, **11**, 7304-7316.
11. W. Zhang, Y. Zou, C. Yu and W. Zhong, *Journal of Power Sources*, 2019, **439**, 227067.
12. X. H. Zhang, H. X. Li, B. Qin, Q. Wang, X. H. Xing, D. H. Yang, L. E. Jin and Q. Cao, *Journal of Materials Chemistry A*, 2019, **7**, 3298-3306.
13. H. Su, H. Zhang, F. Liu, F. Chun, B. Zhang, X. Chu, H. Huang, W. Deng, B. Gu, H. Zhang, X. Zheng, M. Zhu and W. Yang, *Chemical Engineering Journal*, 2017, **322**, 73-81.
14. H. X. Li, S. Ma, H. Q. Cai, H. H. Zhou, Z. Y. Huang, Z. H. Hou, J. J. Wu, W. J. Yang, H. B. Yi, C. P. Fu and Y. F. Kuang, *Energy Storage Mater.*, 2019, **18**, 338-348.
15. Q. Zhang, Y. J. Huang, D. H. Xia, L. L. Hu, P. Li, L. Tan, Y. Y. Wang, C. He, D. Shu and X. Xie, *Environ.-Sci. Nano*, 2019, **6**, 3359-3373.
16. W. Q. Zhao, H. Zhang, J. Liu, L. Xu, H. S. Wu, M. C. Zou, Q. Wang, X. D. He, Y. B. Li and A. Y. Cao, *Small*, 2018, **14**, 10.
17. C. X. Zhou, T. T. Gao, Y. J. Wang, Q. L. Liu, Z. H. Huang, X. X. Liu, M. Q. Qing and D. Xiao, *Small*, 2019, **15**, 15.
18. Y. Li, S. Zheng, X. Liu, P. Li, L. Sun, R. Yang, S. Wang, Z. S. Wu, X. Bao and W. Q. Deng, *Angew Chem Int Ed Engl*, 2018, **57**, 7992-7996.
19. D. Wang, Y. Wang, H. Liu, W. Xu and L. Xu, *Chemical Engineering Journal*, 2018, **342**, 474-483.
20. M. M. Vadiyar, X. Liu and Z. Ye, *ACS applied materials & interfaces*, 2019, **11**,

45805-45817.
21. M. Sevilla and A. B. Fuertes, *ACS Nano*, 2014, **8**, 5069-5078.
22. J. Yang, H. Wu, M. Zhu, W. Ren, Y. Lin, H. Chen and F. Pan, *Nano Energy*, 2017, **33**, 453-461.
23. J. H. Hou, C. B. Cao, F. Idrees and X. L. Ma, *ACS Nano*, 2015, **9**, 2556-2564.
24. D. Wang, S. Liu, L. Jiao, G. Fang, G. Geng and J. Ma, *Carbon*, 2017, **119**, 30-39.
25. X. Shi, S. Zhang, X. Chen, T. Tang and E. Mijowska, *Carbon*, 2020, **157**, 55-63.
26. M. Khalaj, A. Sedghi, H. N. Miankushki and S. Z. Golkhatmi, *Energy*, 2019, **188**, 116088.
27. Y. An, Y. Yang, Z. Hu, B. Guo, X. Wang, X. Yang, Q. Zhang and H. Wu, *Journal of Power Sources*, 2017, **337**, 45-53.